Proceedings of the ASME 2011 International Design Engineering Technical Conferences & Computers and Information in Engineering Conference
IDETC/PTG 2011
August 29-31, 2011, Washington, DC, USA

DETC2011-47759

EFFECTS OF PRELOADS ON VIBRATION TRANSMISSION THROUGH DOUBLE ROW ANGULAR CONTACT BALL BEARINGS

Aydin Gunduz
The Ohio State University
Columbus, Ohio, USA

Jason T. Dreyer
The Ohio State University
Columbus, Ohio, USA

Rajendra Singh
The Ohio State University
Columbus, Ohio, USA

ABSTRACT

This work investigates the role of double row angular contact ball bearings as a vibration transmitter in shaft-bearing assemblies. In our analyses the double row bearings are represented as five dimensional stiffness elements (with associated damping) through an extension of the stiffness matrix concept described by Lim and Singh (1989) for single row bearings to double row angular contact ball bearings. In particular, the effects of bearing preloads on dynamic characteristics of double row angular contact ball bearings are first numerically explored. The dynamic responses of face-to-face, back-to-back and tandem arrangements are evaluated on a comparative basis under various preloads. The nature and extent of preloads significantly affect the vibration characteristics of the bearing assembly due to major changes in the diagonal and off-diagonal elements of the stiffness matrix, and these effects vary for alternate configurations. The dynamic effects of bearing preloads are then experimentally investigated for a wheel bearing assembly containing double row angular contact ball bearings (with back-to-back arrangement) under two different preloading mechanisms. Experiments show that the mechanism and amount of bearing preloads significantly affect the system natural frequencies, mode shapes and vibration amplitudes, thus altering the vibration behavior of the bearing assembly. Suggestions for further work and applications will be briefly mentioned.

1 INTRODUCTION

Literature on double row angular contact ball bearings is sparse though they are widely used in industrial, automotive and aircraft applications such as in gear boxes, wheel hubs, machine tool spindles, industrial pumps and air compressors due to their ease of maintenance, ability to carry bidirectional loads and relatively low cost compared to other double row bearings. Thus the main goal of this paper is to investigate double row angular contact ball bearings as a vibration transmitter and explore the effects of preloads on the dynamics of such shaft-bearing systems. Fig. 1 shows three double row angular contact ball bearing configurations: (i) Back-to-back (DB) or 'O' arrangement (Fig. 1a) in which the load lines (lines passing through the contact point of the rolling elements) meet outside of the bearing; (ii) face-to-face (DF) or 'X' arrangement (Fig. 1b) where the load lines converge toward the bore of the bearing; (iii) tandem (DT) or series arrangement (Fig. 1c) where the load lines act in parallel so they never meet each other as opposed to the other two arrangements. In this paper, the vibratory characteristics of these three arrangements will be briefly evaluated on a comparative basis under various preloads considering alternate damping mechanisms. Results from an experiment are also described.

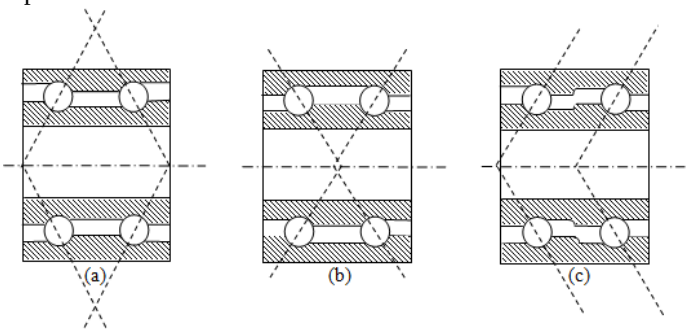

Figure 1. THREE ARRANGEMENTS OF DOUBLE ROW ANGULAR CONTACT BALL BEARINGS: (a) BACK-TO-BACK (DB) OR 'O' ARRANGEMENT; (b) FACE-TO-FACE (DF) OR 'X' ARRANGEMENT; (c) TANDEM (DT) ARRANGEMENT

2 LITERATURE REVIEW

2.1 Preload Issues

The effects of bearing preloads on the performance of shaft-bearing systems and their dynamic characteristics have been studied by several authors [1-3]. Akturk et al. [4] used a three-degree-of-freedom model to study the effects of bearing preload and number of rolling elements on vibration characteristics of an angular contact ball bearing. They observed a reduction in the vibration amplitudes associated with the ball passage frequency with increasing axial preload. Alfares and Elsharkawy [5] made similar observations using a five-degrees-of-freedom model. They also presented a reduction in peak-to-peak amplitudes (in time domain) with increasing preload. Bai et al. [6] used the same five-degree-of-freedom model to observe the nonlinear dynamic characteristics of a rolling element bearing. They showed that unstable periodic solution of a balanced rotor bearing system can be avoided with a sufficient axial preload.

2.2 Bearing Stiffness

Although Jones [7] did not define a bearing stiffness matrix, his load-deflection formulations for ball and roller type bearings under static loading conditions could be used to define a fully populated stiffness matrix for single row bearings. Lim and Singh [8] developed a five dimensional, symmetric bearing stiffness matrix (which is in fact a six dimensional matrix with last column and row being all zeros corresponding to the torsional motions) for a single row spherical contact ball-type and cylindrical contact roller-type bearings. The main advantage of Lim and Singh's stiffness model [8] over the previous models was the introduction of flexural and out-of-plane type motions which provided a better understanding of vibration transmission through rolling element bearings. Lim and Singh showed the validity of their model in their series of papers [8-12] through parametric studies and comparisons with previous analytical and experimental results [13-14]. Cermelj and Boltezar [15] used this stiffness model to further investigate the dynamics of a structure containing ball bearings. Lim and Singh's model has also been utilized by Royston and Basdogan [16] to study the vibration transmission through self-aligning (spherical) bearings where they proposed a stiffness matrix for double row self-aligning bearings. As the moment stiffness of self-aligning bearings are negligible, Royston and Basdogan [16] did not consider the effects angular displacements and tilting moments which normally brings the most of the complexity to systems with multiple row bearings. Thus, their three dimensional stiffness matrix was, in fact, a simplified version of Lim and Singh's five dimensional model [8], where the last two rows and columns of moment stiffness terms are neglected, but three dimensional translational motions of each rolling element of both rows are included.

2.3 Double Row Bearings

Although single row bearings have been well and extensively studied, publications specific to double row bearings are sparse. Bercea et al. [17] formulated the relative displacement between the bearing rings (also termed as the 'ring approach') for various double row bearing types such as tapered, spherical, cylindrical roller and angular contact ball bearings. Their study was limited to a formulation of bearing deflections and did not include any stiffness formulation or dynamic analysis. Then Nelias and Bercea [18] used their double row tapered rolling bearing model for case studies. Cao and Xiao [19] developed a dynamic model for double row spherical roller bearings based on energy principles. Later Cao [20] improved this model by including the effects of rotational motions and shaft misalignments. Choi and Yoon [21] proposed a method for determining the discrete design variables of an automotive wheel assembly that contained a double row angular contact ball bearing.

3 DYNAMIC MODEL

3.1 Bearing Stiffness Model

Our literature survey did not yield any study that analyzes the effects of bearing preloads on the dynamics of shaft-bearing systems with double row angular contact ball bearings. This study fills this gap while presenting new computational and experimental results to provide a better understanding of the preload effects on shaft-bearing dynamics.

In this study, the double row bearings are represented as five dimensional stiffness elements with associated damping through an extension of the stiffness matrix concept described by Lim and Singh [8] for single row bearings to double row angular contact ball bearings. In this model, the outer ring is assumed to be fixed in the space and the inner ring is displaced under loads. The mean bearing load vector $\mathbf{f_m} = \{F_{xm}, F_{ym}, F_{zm}, M_{xm}, M_{ym}\}^{\mathrm{T}}$ is assumed as a point load acting along the geometrical center of the bearing and resulting in the mean displacement vector $\mathbf{q_m} = \{\delta_{xm}, \delta_{ym}, \delta_{zm}, \beta_{xm}, \beta_{ym}\}^{\mathrm{T}}$ as shown in Fig. 2. In our model, one of these two vectors has to be known in order to calculate the five dimensional, symmetric bearing stiffness matrix $\mathbf{K_b}$ as shown below.

$$\mathbf{K_b} = \frac{\partial \mathbf{f_m}}{\partial \mathbf{q_m}} = \begin{bmatrix} k_{xx} & k_{xy} & k_{xz} & k_{x\theta_x} & k_{x\theta_y} \\ & k_{yy} & k_{yz} & k_{y\theta_x} & k_{y\theta_y} \\ & & k_{zz} & k_{z\theta_x} & k_{z\theta_y} \\ & \textit{symmetric} & & k_{\theta_x\theta_x} & k_{\theta_x\theta_y} \\ & & & & k_{\theta_y\theta_y} \end{bmatrix} \quad (1)$$

Mathematical formulation of $\mathbf{K_b}$ will not be outlined in this paper, however the model can be summarized in terms of inputs and outputs as shown in Fig. 3 for a given $\mathbf{q_m}$ or $\mathbf{f_m}$.

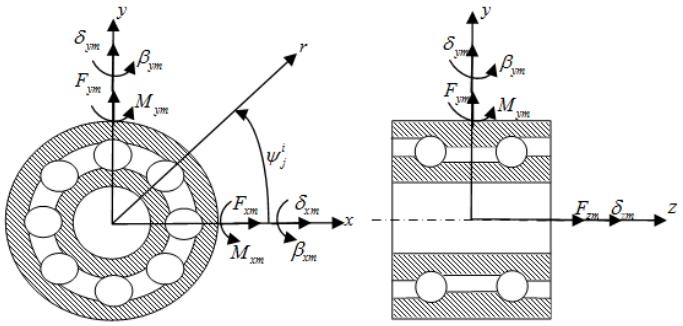

Figure 2. MEAN LOADS AND MOMENTS ON THE BEARING AND RESULTING TRANSLATIONAL AND ROTATIONAL DISPLACEMENTS. THE COORDINATE SYSTEM IS ALSO SHOWN

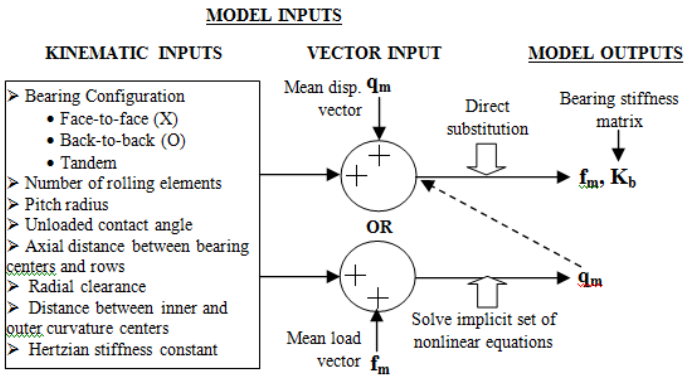

Figure 3. THE SUMMARY OF THE STIFFNESS MATRIX MODEL IN TERMS OF SYSTEM INPUTS AND OUTPUTS

3.2 Lumped Parameter Model

Since our main purpose is to investigate the effects of bearing preloads on the bearing stiffness matrix elements and consequent effects on vibration transmitter characteristics of double row angular contact ball bearings, we will neglect shaft and casing compliances in our numerical analyses. This facilitates the creation of a simple, five dimensional lumped parameter model as shown in Fig. 4 where a rigid shaft $(\mathbf{M_S})$ is supported by a double row angular contact ball bearing represented as a five dimensional bearing stiffness matrix ($\mathbf{K_b}$ with an associated $\mathbf{C_b}$) that is directly connected to the ground. This linear, time-invariant, multi-degree-of-freedom vibratory model can be written in matrix form as

$$\mathbf{M}\ddot{\mathbf{x}}(t)+\mathbf{C}\dot{\mathbf{x}}(t)+\mathbf{K}\mathbf{x}(t)=\mathbf{f}(t) \qquad (2)$$

where $\mathbf{M}$, $\mathbf{C}$ and $\mathbf{K}$ are system mass, viscous damping and stiffness matrices respectively, $\mathbf{f}(t)$ is the external dynamic force vector and $\mathbf{x}(t)$ is the displacement response vector. Note the bearing preloads do not explicitly appear in Eq. (2).

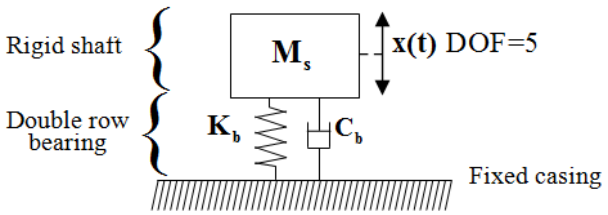

Figure 4. FIVE DEGREES-OF-FREEDOM LUMPED PARAMETER MODEL

However, they dictate the vibration characteristics of the bearing system via diagonal and off-diagonal terms of $\mathbf{K_b}$ (as well as elements of $\mathbf{C_b}$). Mass, damping and stiffness matrices of the shaft-bearing system become $\mathbf{M}=\mathbf{M_S}$, $\mathbf{C}=\mathbf{C_b}$ and $\mathbf{K}=\mathbf{K_b}$ where

$$\mathbf{M_S}=\begin{bmatrix} m_s & 0 & 0 & 0 & 0 \\ 0 & m_s & 0 & 0 & 0 \\ 0 & 0 & m_s & 0 & 0 \\ 0 & 0 & 0 & I_{xx} & I_{xy} \\ 0 & 0 & 0 & I_{yx} & I_{yy} \end{bmatrix} \qquad (3)$$

and $\mathbf{K_b}$ is given by Eq. (1). The damping matrix, however, can not be easily predicted due to unknown damping characteristics of rolling element bearings [9]. The damping for rolling element bearings must be found from experimental results. For a nonproportionally damped MDOF system Eq. (2) can be rewritten by defining a state vector $\mathbf{q}(t)=(\dot{\mathbf{x}}(t),\mathbf{x}(t))^T$ as:

$$\begin{bmatrix} \mathbf{M} & \mathbf{C} \\ \mathbf{0} & \mathbf{M} \end{bmatrix}\begin{Bmatrix} \ddot{\mathbf{x}} \\ \dot{\mathbf{x}} \end{Bmatrix}+\begin{bmatrix} \mathbf{0} & \mathbf{K} \\ -\mathbf{M} & \mathbf{0} \end{bmatrix}\begin{Bmatrix} \dot{\mathbf{x}} \\ \mathbf{x} \end{Bmatrix}=\begin{Bmatrix} \mathbf{f} \\ \mathbf{0} \end{Bmatrix} \qquad (4)$$

This is of the form $\mathbf{B}\dot{\mathbf{q}}(t)+\mathbf{A}\mathbf{q}(t)=\mathbf{0}$ where

$$\mathbf{B}=\begin{bmatrix} \mathbf{M} & \mathbf{C} \\ \mathbf{0} & \mathbf{M} \end{bmatrix};\ \mathbf{A}=\begin{bmatrix} \mathbf{0} & \mathbf{K} \\ -\mathbf{M} & \mathbf{0} \end{bmatrix} \qquad (5a\text{-}b)$$

Assuming a solution of the form $\mathbf{q}(t)=\mathbf{v}\exp(\lambda t)$ $(\mathrm{Re}(\lambda)<0)$, gives the generalized eigenvalue problem:

$$\mathbf{A}\mathbf{v}=-\lambda\mathbf{B}\mathbf{v} \qquad (6)$$

The solution of this eigenvalue problem results in 10 eigenvalues and eigenvectors occurring in complex conjugate pairs. The eigenvalue (λ_r) of the rth mode is written as

$$\lambda_r=-\zeta_r\omega_r\pm j\omega_r\sqrt{1-\zeta_r} \qquad (7)$$

and the natural frequencies (ω_r) and damping ratios (ζ_r) of the system can be calculated as:

$$\omega_r = \sqrt{\left(\mathrm{Re}(\lambda_r)\right)^2 + \left(\mathrm{Im}(\lambda_r)\right)^2} \tag{8}$$

$$\zeta_r = \frac{\left|\mathrm{Re}(\lambda_r)\right|}{\sqrt{\left(\mathrm{Re}(\lambda_r)\right)^2 + \left(\mathrm{Im}(\lambda_r)\right)^2}} \tag{9}$$

3.3 Transfer Functions

After constructing the dynamic model, the transfer functions of the vibratory system can be calculated. Evaluating the vibration characteristics of a system with transfer functions is convenient, especially in experimental modal analysis as the accelerance spectra can be easily measured using an impulse hammer test.

The accelerance matrix $\mathbf{A}(\omega)$ can be expressed in the form of system matrices as:

$$\mathbf{A}(\omega) = -\omega^2[-\omega^2\mathbf{M} + j\omega\mathbf{C} + \mathbf{K}]^{-1} \tag{10}$$

which can be written in the following form of (note that all elements of a symmetric matrix are functions of ω):

$$\mathbf{A}(\omega) = \begin{bmatrix} \mathbf{A}_{xx} & \mathbf{A}_{xy} & \mathbf{A}_{xz} & \mathbf{A}_{x\theta_x} & \mathbf{A}_{x\theta_y} \\ & \mathbf{A}_{yy} & \mathbf{A}_{yz} & \mathbf{A}_{y\theta_x} & \mathbf{A}_{y\theta_y} \\ & & \mathbf{A}_{zz} & \mathbf{A}_{z\theta_x} & \mathbf{A}_{z\theta_y} \\ & \textit{symmetric} & & \mathbf{A}_{\theta_x\theta_x} & \mathbf{A}_{\theta_x\theta_y} \\ & & & & \mathbf{A}_{\theta_y\theta_y} \end{bmatrix} \tag{11}$$

4 ILLUSTRATIVE EXAMPLE

Consider a shaft-bearing assembly with a commercial double row angular contact ball bearing whose properties are given in Tab. 1. These properties are either given by the manufacturer or determined by kinematics with the exception of Hertzian stiffness constant which is calculated by an empirical relation [1]. All three bearing configurations (face-to-face, back-to-back and tandem) are considered and the bearing is assumed to be connected to the ground. Thus, the shaft-bearing system can be represented by the lumped parameter model shown in Fig. 4 assuming rigid shaft which has a mass of m_s = 5 kg, and an inertia of $I_{xx} = I_{yy}$ = 0.0144 kgm^2. Here we will assume that the cross-coupling inertia terms of the shaft are negligible ($I_{xy} = I_{yx} = 0$) that results in a diagonal mass matrix.

As far as the viscous damping matrix is concerned a diagonal matrix is initially employed based on experimental results (to be discussed more in detail in the next section) that is kept constant for all preloads. The matrix if of the form:

Table 1. KINEMATIC PROPERTIES OF THE EXAMPLE CASE

Property	Symbol (unit)	Value
Total number of rolling elements	Z	26 (13x2)
Radial clearance	r_L (mm)	0
Hertzian stiffness constant	K_n (N/mm$^{1.5}$)	414,000
Radius of the inner raceway groove curvature center (pitch radius)	R (mm)	31.75
Unloaded distance between inner and outer raceway groove curvature	A_o (mm)	0.55
Axial distance between the geometric center and bearing one row	e (mm)	18.20
Unloaded contact angle	α_o (deg)	35
Load-deflection exponent	n	1.5

$$\mathbf{C_b} = diag\left([c_{xx},\ c_{yy},\ c_{zz},\ c_{\theta_x\theta_x},\ c_{\theta_y\theta_y}]\right) \tag{12}$$

where $c_{xx} = c_{yy} = c_{zz}$ =5000 Ns/m and $c_{\theta_x\theta_x} = c_{\theta_y\theta_y} = 1$ Nms/rad.

In this numerical example we will demonstrate the effects of axial preloads although other loading scenarios could be easily applied. In the absence of any external radial or moment loads on the bearing the only significant off-diagonal terms of the bearing stiffness matrix are $k_{x\theta_y}$ and $k_{y\theta_x}$ (and their symmetric elements $k_{\theta_y x}$ and $k_{\theta_x y}$), which provide a coupling between the translational and rotational degrees of freedom in two radial directions, x and y. Also, the translational and rotational stiffness coefficients in x and y directions are identical to each other ($k_{xx} = k_{yy}$, $k_{\theta_x\theta_x} = k_{\theta_y\theta_y}$), which causes an overlap in relevant system modes for a pure axial loading. For our particular example, the first and the second (radial) modes, and the fourth and the fifth (tilting) modes are identical to each other. The third mode that corresponds to axial translational vibrations is a unique mode and uncoupled from all other modes because all the z-axis related off-diagonal terms are negligible when there is no radial or moment loads on the bearing.

The natural frequencies of the shaft-bearing system with respect to axial preload are illustrated in Fig. 5(a-c) for face-to-face, back-to-back and tandem arrangements respectively. An increase in the axial preload from 1 kN to 20 kN, affects the diagonal and off-diagonal terms of the stiffness matrix and increases the system natural frequencies for all arrangements as can be seen from the figure. However these values show considerable variations among the three arrangements. For

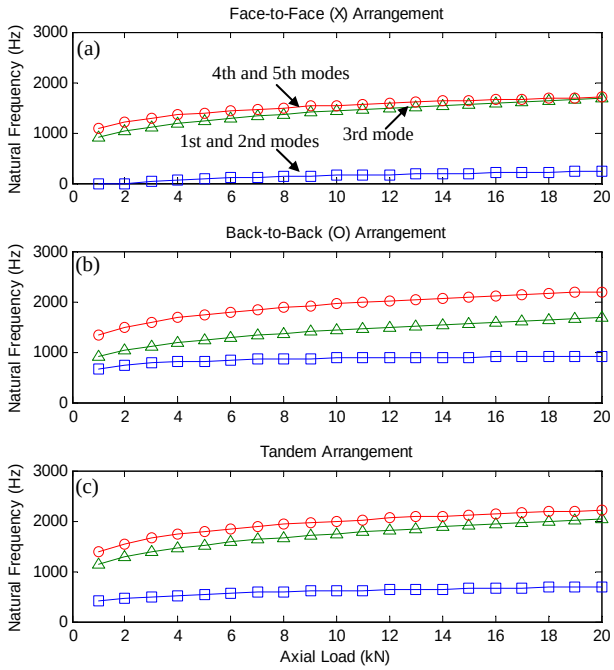

Figure 5. NATURAL FREQUENCIES OF THE NUMERICAL EXAMPLE WITH INCREASING AXIAL PRELOAD. (a) FACE-TO-FACE (X) ARRANGEMENT, (b) BACK-TO-BACK (O) ARRANGEMENT, (c) TANDEM ARRANGEMENT. KEY: (□), FIRST AND SECOND MODES; (△), THIRD MODE; (○) FOURTH AND FIFTH MODES

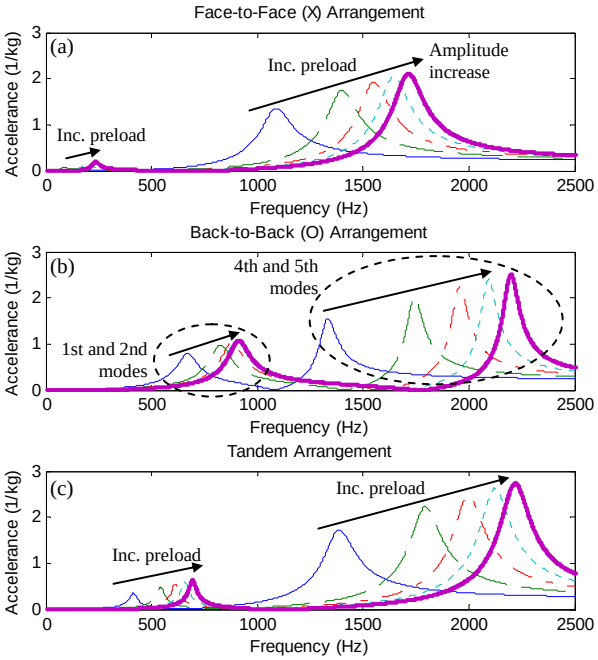

Figure 6. RADIAL ACCELERANCE MAGNITUDE SPECTRA $\left|\mathbf{A}_{xx}(\omega)\right|$ OF THE NUMERICAL EXAMPLE WITH CONSTANT NON-PROP. DAMPING FOR VARIOUS AXIAL PRELOADS, (a) FACE-TO-FACE (X) ARRANGEMENT, (b) BACK-TO-BACK (O) ARRANGEMENT, (c) TANDEM ARRANGEMENT. KEY: AXIAL PRELOAD; (——), 1 kN; (— -), 5 kN; (– ·) 10 kN; (·····) 15 kN; (▬) 20 kN.

example, the first overlapped mode of face-to-face arrangement occur at a very low frequency that it does not even have a real value until the axial preload is increased to 3 kN. Above 3 kN, this mode still remains at a low frequency regime (between 1-200 Hz), whereas the same mode occurs between 700-900 Hz for back-to-back arrangement. This mode for tandem arrangement occurs between those of the other two arrangements in 400-600 Hz range. This result could be explained by the fact that back-to-back arrangement, which is designed to carry heavier moment loads, have higher moment stiffness terms ($k_{\theta_x\theta_x}$ and $k_{\theta_y\theta_y}$) that considerably increases the natural frequencies of the angular (tilting) modes. Since the radial modes are highly coupled with the tilting modes through the cross-coupling terms ($k_{x\theta_y}$ and $k_{y\theta_x}$), the overlapped radial mode of back-to-back arrangement also occur at a higher frequency although the radial stiffness coefficients ($k_{xx} = k_{yy}$) are the same for face-to-face and back-to-back arrangements under a pure axial load. Conversely, the face-to-face arrangement, which is designed to provide a better compensation for shaft misalignments (which are closer to self-aligning bearings in this sense) have much lower tilting stiffness coefficients due to the shortness of its effective load center. This lowness of the tilting stiffness coefficients causes the resonances to occur at much lower frequencies.

The axial vibration mode (the third mode), however, occurs at the exact same frequencies for face-to-face and back-to-back arrangements (which is ranging from 900 to 1400 Hz with increasing preload) as they show the same vibration behavior in axial direction. This is because their axial stiffness coefficients (k_{zz}) are the same and there is no coupling between the tilting and axial modes ($k_{z\theta_x} = k_{z\theta_y} = 0$) in the absence of any radial or moment loads. However, if the rolling elements are arranged in tandem configuration, this axial mode occurs at a higher natural frequency (between 1100-1800 Hz) due to the high axial rigidity of tandem configuration (of course we assume the tandem arrangement is loaded in the direction it can carry).

Observation of the system transfer functions at selected preloads could give us more information on the vibration characteristics of shaft-bearing system. Thus the radial accelerance magnitude spectra ($\left|\mathbf{A}_{xx}(\omega)\right|$) is plotted for five different axial preloads (1, 5, 10, 15, 20 kN) in Fig. 6(a-c) for face-to-face, back-to-back and tandem arrangements respectively. The plots clearly illustrate the shift of resonance frequencies towards right with increasing axial preloads. Again, one can observe that the back-to-back arrangement has the highest resonance frequencies followed by tandem and face-to-face configurations respectively. If the vibration amplitudes are to be sorted from maximum to minimum, the same exact order

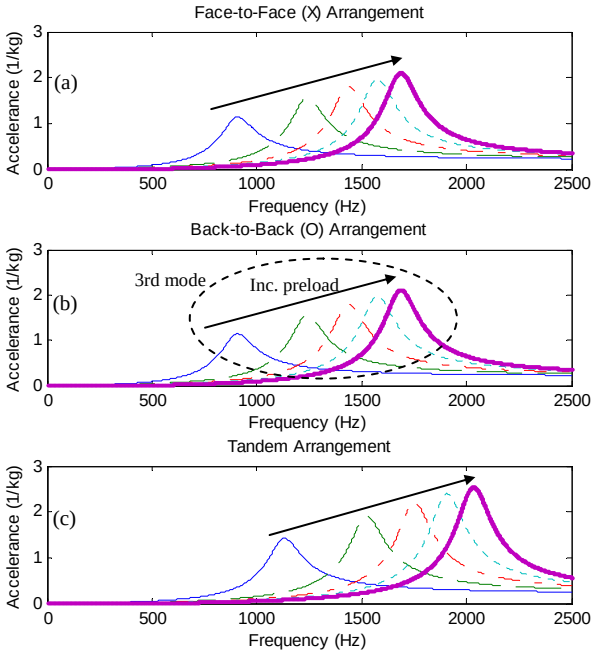

Figure 7. AXIAL ACCELERANCE MAGNITUDE SPECTRA $\left|\mathbf{A}_{zz}(\omega)\right|$ OF THE NUMERICAL EXAMPLE WITH CONSTANT NON-PROPORTIONAL DAMPING FOR VARIOUS AXIAL PRELOADS, (a) FACE-TO-FACE (X) ARRANGEMENT, (b) BACK-TO-BACK (O) ARRANGEMENT, (c) TANDEM ARRANGEMENT. KEY: AXIAL PRELOAD; (——), 1 kN; (— -), 5 kN; (– ·) 10 kN; (·····) 15 kN; (▬) 20 kN.

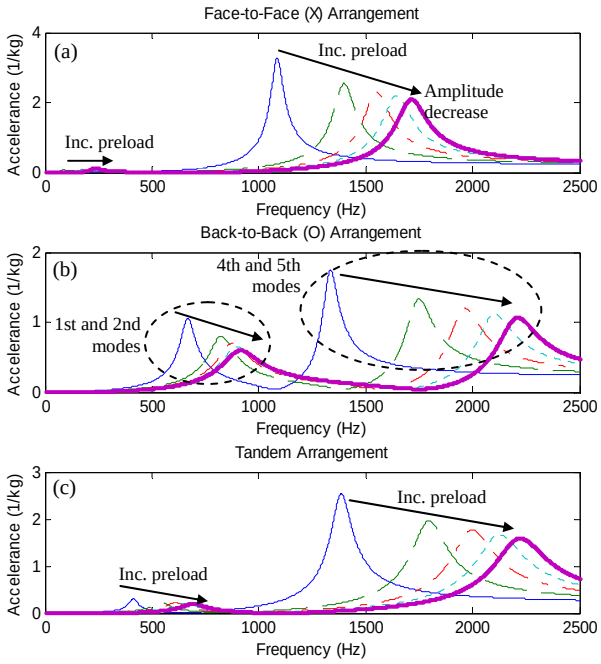

Figure 8. RADIAL ACCELERANCE MAGNITUDE SPECTRA $\left|\mathbf{A}_{xx}(\omega)\right|$ OF THE NUMERICAL EXAMPLE WITH PROPORTIONAL DAMPING FOR VARIOUS AXIAL PRELOADS, (a) FACE-TO-FACE (X) ARRANGEMENT, (b) BACK-TO-BACK (O) ARRANGEMENT, (c) TANDEM ARRANGEMENT. KEY: AXIAL PRELOAD; (——), 1 kN; (— -), 5 kN; (– ·) 10 kN; (·····) 15 kN; (▬) 20 kN.

of bearing configurations applies (which is especially clear for the first overlapped mode). It is also apparent that these peak amplitudes are growing with increasing axial preload when a constant non-proportional damping matrix described by Eq. (12) is selected.

Since the axial vibration mode (the third mode) is uncoupled from other modes of vibration, its resonant peak cannot be seen in the radial accelerance spectra. In order to observe this mode, the axial accelerance magnitude spectra $\left(\left|\mathbf{A}_{zz}(\omega)\right|\right)$ are plotted in Fig. 7(a-c). As expected, face-to-face and back-to-back arrangements have an identical spectrum, whereas this mode occurs at a higher frequency with higher amplitudes for tandem configuration. The vibration amplitudes are still increasing with an increase in axial preload.

Now, let us consider a case where the damping matrix is proportional to the stiffness matrix with a proportionality constant σ as given in Eq. (13), hence, it is affected by the preload changes as opposed to the constant damping assumption while all other parameters are kept the same.

$$\mathbf{C}_{\mathbf{b}} = \sigma \mathbf{K}_{\mathbf{b}}, \quad \text{where} \quad \sigma = 10^{-7} \text{ s} \qquad (13)$$

If we now view the radial and axial accelerance spectra $\left(\left|\mathbf{A}_{xx}(\omega)\right| \text{ and } \left|\mathbf{A}_{zz}(\omega)\right|\right)$ which are shown in Figs. 8(a-c) and 9(a-c) respectively, we observe that the peak magnitudes at

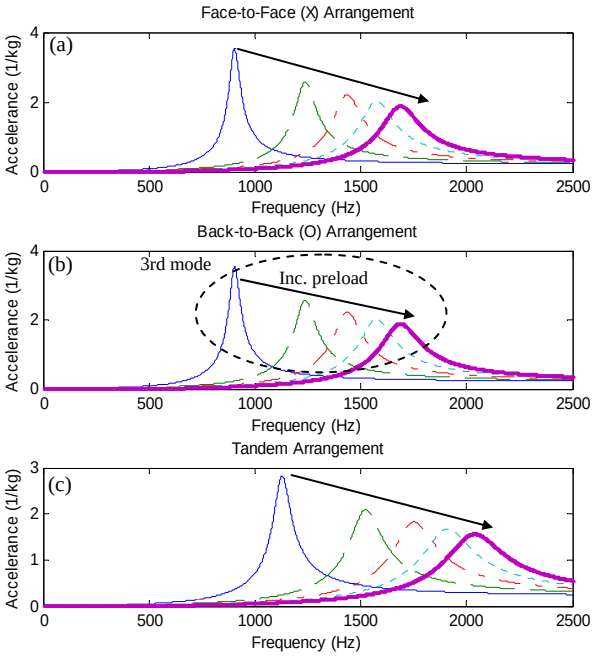

Figure 9. AXIAL ACCELERANCE MAGNITUDE SPECTRA $\left|\mathbf{A}_{zz}(\omega)\right|$ OF THE NUMERICAL EXAMPLE WITH PROPORTIONAL DAMPING FOR VARIOUS AXIAL PRELOADS, (a) FACE-TO-FACE (X) ARRANGEMENT, (b) BACK-TO-BACK (O) ARRANGEMENT, (c) TANDEM ARRANGEMENT. KEY: AXIAL PRELOAD; (——), 1 kN; (— -), 5 kN; (– ·) 10 kN; (·····) 15 kN; (▬) 20 kN.

all modes decrease with increasing axial preload as opposed to the previous case. The peak amplitudes corresponding to light preloads (such as 1 kN) are considerably elevated; whereas they are reduced for heavy preloads (such as 20 kN). Another observation here is that even though the natural frequencies do not show significant variations, the shapes of the peaks are considerably altered when compared with the viscous damping mechanism described by Eq. (12).

Since the damping characteristics of rolling element bearings are not very well understood, numerical consideration of these alternate damping mechanisms is important as it will assist us to interpret damping behavior of the experimental results as discussed in the following section.

5 EXPERIMENTAL STUDY

5.1 Experimental Setup

A test setup composed of an automotive wheel-hub assembly, shown in Fig. 10 schematically, is designed to experimentally analyze the effects of bearing preloads. The shaft is supported by a wheel bearing, which is a double row angular contact ball bearing with back-to-back arrangement. The bearing housing (the knuckle for this case), is rigidly clamped to a pedestal that is rigidly connected to the ground. The experiment is conducted at static conditions to avoid any rotational effects that have been well studied by several authors [22-24]. The bearing is initially unloaded in the axial direction. The initial radial preload is given in terms of radial clearance that is between 0 and -30 μm (note that this negative clearance defines a displacement preload); which creates some uncertainty on the initial radial preload. Additional bearing preloads are applied via the following mechanisms.

1. Axial preload: Applied through the shaft by tightening the nuts at both ends of threaded rod inside the shaft that can be seen in Fig. 10. The applied load is measured with a washer type load cell that is placed between one of the nuts and flange on the shaft.

2. Radial + moment load: Applied as a static shaft load using a hydraulic jack that is placed on a stable base as shown in Fig. 10. The applied radial load, which is carried by the wheel bearing, essentially imposes a moment load on the bearing as well. The amount of preload is measured with a button-type load cell attached at the top of the jack.

An impulse hammer test has been conducted at various axial and radial preloads and accelerance measurements are taken for numerous impact and accelerometer locations. In these measurements the angular position of the shaft (and essentially the bearing) are kept the same for all preloads. In this paper we will present sample results for the case when a triaxial accelerometer is attached right end of the shaft and the impact is on the left end of the shaft in axial direction (as illustrated in Fig. 10).

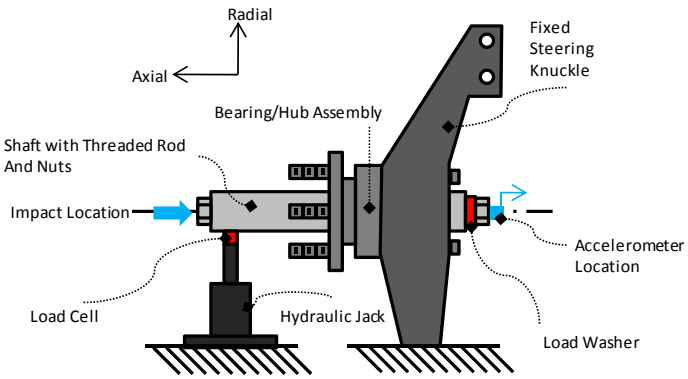

Figure. 10. EXPERIMENTAL STUDY WITH WHEEL-HUB ASSEMBLY SETUP AND ILLUSTRATION OF PRELOADING MECHANISMS OF THE SYSTEM UTILIZING HYDRAULIC JACK (FOR RADIAL DIRECTION) AND SHAFT WITH THREADED ROD (FOR AXIAL PRELOADING)

5.2 Effects of Axial Preload

Axial preloads ranging from 0.45 kN to 2.67 kN have been applied with 0.22 kN increments, and the accelerance data have been collected at each preload. These preloads are within $\pm$ 0.05 kN error margin as it is not possible to apply an exact amount of preload with the explained nature of preloading.

Typical accelerance magnitude measurements are plotted in Fig. 11 up to 4000 Hz for all preloads. The first natural frequency, which is magnified in Fig. 11(b), shifts gradually from 660 Hz to 810 Hz as the applied preload increases from 0.45 kN to 2.67 kN. Also the peak magnitude of this mode significantly reduces with increasing axial preload, which has a resemblance to the proportional damping case discussed in the previous section. We can observe another mode around 900 Hz, with much lower amplitudes and shifts slightly towards right with increasing axial preload.

Another vibration mode can be observed around 1620 Hz. Although this mode does not exhibit a considerable frequency shift, its amplitude is significantly attenuated with an increase in axial preload. This mode predominantly corresponds to the axial vibrations of the shaft which is consistent with the illustrative example of section 4. A reduction in the vibration amplitude can be explained by the fact that a high preload overcomes the axial clearance within the bearing and consequently does not permit axial vibrations of the shaft. Conversely, when axial preload is low, high amplitude vibrations seem to occur due to a higher clearance.

The next resonant peak shifts from 1890 Hz to 2120 Hz when axial preload is increased from 0.45 kN to 2.67 kN. This mode represents a combination of tilting motions of the shaft and radial vibrations. Note that at lower preloads, more than one peak is seen in this frequency range. The amplitude at this mode also attenuates with increasing preloads and totally diminishes for preloads higher than 2.22 kN. Measurements described so far seem to suggest an increase in the damping ratios with increasing axial preload which is similar to the proportional damping case described by Eq. (13).

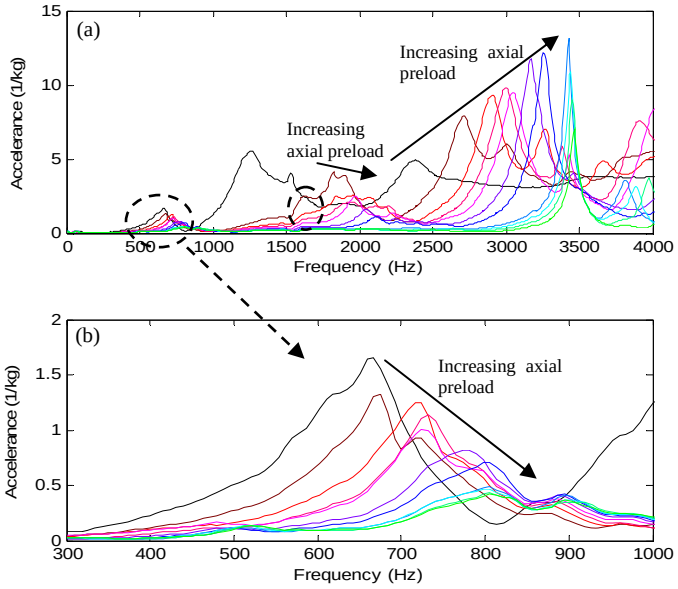

Figure 11. ACCELERANCE MAGNITUDE SPECTRA MEASURED FOR VARIOUS AXIAL PERLOADS. KEY: AXIAL PRELOAD; (—), 0.45 kN; (—), 0.67 kN; (—), 0.89 kN; (—), 1.11 kN; (—), 1.33 kN; (—), 1.56 kN; (—), 1.78 kN; (—), 2.00 kN; (—), 2.22 kN; (—) 2.45 kN; (—)2.67 kN;

The largest peak of the system starts at 2400 Hz for 0.45 kN of preload and shifts gradually towards 3500 Hz as the axial preload increases. However the vibration amplitudes of this mode significantly increases with increasing preload as opposed to previous modes, showing a resemblance with the first damping mechanism considered in our numerical example. This peak reaches its maximum amplitude when the preload is 2.00 kN, and then starts to decay in amplitude for higher preloads without a significant frequency shift. This shows that the accelerance curves start to show some deviations from the general trends at excessive axial preloads.

5.3 Effects of Radial + Moment Load

The effects of radial preloads (+ bending moments) is investigated following the same procedure. Before the application of the radial preload, the axial preload is set to 2.67 kN, which is significantly affected by the applied radial + moment load. A radial preload ranging from 0.89 kN to 4.44 kN is applied with 0.44 kN increments, and the accelerance data is collected utilizing the same impact and accelerometer locations.

Fig. 12 illustrates the accelerance magnitude spectra at each radial preload. The shifts in the transfer functions show a very clear trend with increasing preload, however the direction of the shifts are different for each mode.

A unique characteristic of this case is that the first mode, which occurs in the 600-800 Hz range, is shifting towards left instead of right, showing a reduction in the resonance frequency with increasing radial load. This unexpected behavior could be caused due to a relief in the axial preload when the bending moment is simultaneously imposed on the

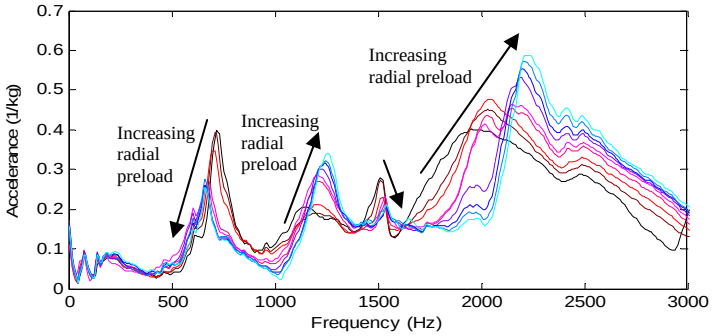

Figure 12. ACCELERANCE MAGNITUDE SPECTRA FOR VARIOUS RADIAL PRELOADS. KEY: RADIAL PRELOAD; (—), 0.89 kN; (—), 1.33 kN; (—) 1.78 kN; (—) 2.22 kN; (—) 2.67 kN; (—), 3.11 kN; (—), 3.55 kN; (—) 4.00 kN; (—) 4.44 kN;

bearing. Other modes do not display this behavior as they shift towards right with increasing radial load due to an increase in the stiffness coefficients as expected. The second mode, which was not very obvious in previous axial preloading case, now occur around 1200-1300 Hz with considerable amplitudes that are increasing with increasing radial load as opposed to the first mode. The axial vibration mode now occurs around 1500 Hz, within a much narrower band and the trend of the shift is towards right and down with increasing radial load. A combination of tilting and radial (translational) mode occurring within 2000-2500 Hz band now shifts right and upwards with increasing radial load.

Some of the observations from preliminary experimental studies could be summarized as follows:

- Changes in the system preloads result in clear shifts of the accelerance spectrum due to changes in the stiffness and damping characteristics of the system. These shifts could be utilized in preload monitoring applications.
- These shifts display a mode-dependent behavior. In general, as the preload increases the resonance frequencies of the shaft-bearing system shifts towards right due to the increase in bearing stiffness elements. However, the first mode of the system does not obey this generalization when the system is radially preloaded.
- The vibration amplitudes of certain modes attenuate, whereas the others amplify with increasing axial or radial preloads. This suggests a mode-dependent damping mechanism. Such complicated damping characteristics of the rolling element bearings would require further investigation.

6 CONCLUSION

The effects of bearing preloads on the vibration characteristics of shaft-bearing systems with double row angular contact ball bearings have been analyzed in this study. First, the effects of axial preloads are numerically investigated

on a shaft-bearing assembly containing a double row angular contact ball bearing. In these analyses the bearings are represented as five dimensional stiffness elements (with associated damping) through an extension of the stiffness matrix concept described by Lim and Singh [8]. Second, the vibration characteristics of face-to-face, back-to-back and tandem arrangements are evaluated on a comparative basis. Analyses show that the resonant frequencies of back-to-back arrangement that are related to radial and tilting vibration occur at higher frequencies due to its larger moment stiffness terms. Similarly, the axial vibration frequency of the tandem arrangement is higher than the other two configurations due to its high axial stiffness. Third, two different damping mechanisms are investigated in this study. The first one is a viscous damping matrix which kept constant for all preloads resulted in increasing vibration amplitudes with increasing axial preload. The second one is a proportional damping case, which resulted in reducing vibration amplitudes with increasing preload.

The dynamic effects of bearing preloads are then experimentally investigated for a wheel bearing assembly containing double row angular contact ball bearings (with back-to-back arrangement) under two different preloading mechanisms. First, studies are conducted under axial preloads; then radial + moment loads are applied. It is observed that each vibratory mode responds differently to the changes in axial or radial preloads.

The current efforts include development of a preload dependent dynamic model of the experiment based on these measurements. Initial efforts are very encouraging as they are able to accurately estimate the natural frequencies. Also experimental modal measurements are in agreement with the numerical model. However, damping characteristics of each mode is yet to be fully understood. Future work should resolve this issue, by employing a frequency dependent damping model, or by using piecewise damping functions.

ACKNOWLEDGMENTS

We are grateful to the member organizations of the Smart Vehicle Concepts Center (www.SmartVehicleCenter.org) and the National Science Foundation Industry/University Cooperative Research Centers program (www.nsf.gov/eng/iip /iucrc) for supporting this work.

REFERENCES

[1] Harris, T.A., 1966. “An analytical method to prevent skidding in high speed roller bearings”. *Tribology Transactions,* **9** (3), pp. 229-241

[2] Wardle, F.P., Lacey, S.J., Poon S.Y., 1983. “Dynamic and static characteristics of a wide speed range machine tool spindle”. *Precision Engineering,* **5** (4), pp. 175-183.

[3] Kim, K., Kim, S.S., 1989. “Effect of preload on running accuracy of spindle”. *International Journal of Machine Tools and Manufacture,* **29** (1), pp. 99-105.

[4] Akturk, N., Uneeb, M., Gohar, R., 1997. “The effects of number of balls and preload on vibrations associated with ball bearings”. *Transactions of the ASME, Journal of Tribology,* **119**, pp. 747-752.

[5] Alfares M., Elsharkawy A.A., 2003. “Effects of axial preloading of angular contact ball bearings on the dynamics of a grinding machine spindle system”. *Journal of Materials Processing Technology,* **136**, pp. 48-59.

[6] Bai C., Zhang H., Xu Q., 2008. “Effects of axial preload of ball bearing on the nonlinear dynamic characteristics of a rotor-bearing system”. *Nonlinear Dynamics,* **53**, pp. 173-190.

[7] Jones A.B., 1960. “A general theory for elastically constrained ball and radial roller bearings under arbitrary load and speed conditions”. *Transactions of the ASME, Journal of Basic Engineering,* **82**, pp. 309-320

[8] Lim T.C., Singh R., 1990. “Vibration transmission through rolling element bearings, part I: bearing stiffness formulation”. *Journal of Sound and Vibration,* **139** (2), pp. 179–199.

[9] Lim T.C., Singh R., 1990. “Vibration transmission through rolling element bearings, part II: system studies”. *Journal of Sound and Vibration,* **139** (2), pp. 201–225.

[10] Lim T.C., Singh R., 1991. “Vibration transmission through rolling element bearings, part III: geared rotor system studies”. *Journal of Sound and Vibration,* **151** (1), pp. 31–54.

[11] Lim T.C., Singh R., 1992. “Vibration transmission through rolling element bearings, part IV: statistical energy analysis”. *Journal of Sound and Vibration,* **153** (1), 37-50.

[12] Lim T.C., Singh R., 1994. “Vibration transmission through rolling element bearings, part V: effect of distributed contact load on roller bearing stiffness matrix”. *Journal of Sound and Vibration,* **169** (4), pp. 547–553.

[13] White M.F., 1979. “Rolling element bearing vibration characteristics: effect of stiffness”. *Journal of Applied Mechanics,* **46** pp. 677-684.

[14] Kraus J., Blech J.J., Braun S.G. 1987. “In situ determination of rolling bearing stiffness and damping by modal analysis”. *Journal of Sound and Vibration, Acoustics, Stress, and Reliability in Design, Transactions of the American Society of Mechanical Engineers,* **109**, pp. 235-240.

[15] Cermelj P., Boltezar M., 2004. “An indirect approach investigating the dynamics of a structure containing ball bearings”. *Journal of Sound and Vibration,* **276** (1-2), pp. 401–417.

[16] Royston T.J., Basdogan I., 1998. “Vibration transmission through self-aligning (spherical) rolling element bearings: theory and experiment”. *Journal of Sound and Vibration,* **215** (5), pp. 997-1014.

[17] Bercea I., Nelias D., Cavallaro G., 2003. “A unified and simplified treatment of the non-linear equilibrium problem of double-row bearings. Part I: rolling bearing model”, *Proceedings of the Institution of Mechanical Engineers, Part J: Journal of Engineering Tribology*, **217** (3), pp. 205-212.

[18] Nelias D., Bercea I., 2003. “A unified and simplified treatment of the non-linear equilibrium problem of double-row bearings. Part II: application to taper rolling bearings supporting a flwxible shaft”. *Proceedings of the Institution of Mechanical Engineers, Part J: Journal of Engineering Tribology*, **217** (3), pp. 213-221.

[19] Cao M., Xiao J., 2008. “A comprehensive dynamic model of double-row spherical roller bearing – model development and case studies on surface defects, preloads, and radial clearance”. *Mechanical Systems and Signal Processing,* **22**, pp. 467-489.

[20] Cao M., 2007. “A refined double-row spherical roller bearing model and its application in performance assessment of moving race

shaft misalignments". *Journal of Vibration and Control*, **13** pp. 1145-1168

[21] Choi D.H., Yoon K.C., 2001. "A design method of an automotive wheel-bearing unit with discrete design variables using genetic algorithms". *Journal of Tribology*, **123**, pp. 181-187.

[22] Jorgensen B.R., Shin Y.C., 1998. "Dynamics of spindle-bearing systems at high speeds including cutting load effects". *Journal of Manufacturing Science and Engineering*, **120**, pp. 387-394.

[23] Tiwari M., Gupta K., Prakash O., 2000. "Dynamic response of an unbalanced rotor supported on ball bearings". *Journal of Sound and Vibration*, **238** (5) pp. 757-779.

[24] Lin C.W., Tu J.F., Kamman J., 2003. "An integrated thermo-mechanical-dynamic model to characterize motorized machine tool spindles during very high speed rotation". *International Journal of Machine Tools and Manufacture*, **43** (10) pp. 1035-1050